Assessing the Cypress Sandstone for Carbon Dioxide-Enhanced Oil Recovery and Carbon Storage: Part II—Leveraging Geologic Characterization to Develop a Representative Geocellular Model for Noble Oil Field, Western Richland County, Illinois

Nathan P. Grigsby and Nathan D. Webb

Illinois State Geological Survey, Prairie Research Institute, University of Illinois at Urbana-Champaign

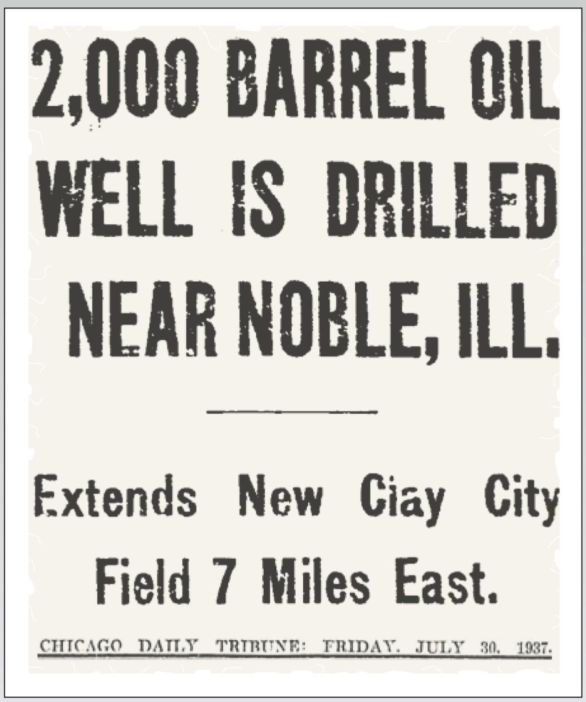

2,000 BARREL OIL WELL IS DRILLED NEAR NOBLE, ILL.

Extends New Clay City Field 7 Miles East.

CHICAGO DAILY TRIBUNE: FRIDAY, JULY 30, 1937.

Circular 602   2020

ILLINOIS STATE GEOLOGICAL SURVEY
Prairie Research Institute
University of Illinois at Urbana-Champaign

ILLINOIS
Illinois State Geological Survey
PRAIRIE RESEARCH INSTITUTE

Front cover: *Headline in the Chicago Daily Tribune, July 30, 1937.*

Assessing the Cypress Sandstone for Carbon Dioxide-Enhanced Oil Recovery and Carbon Storage: Part II—Leveraging Geologic Characterization to Develop a Representative Geocellular Model for Noble Oil Field, Western Richland County, Illinois

Nathan P. Grigsby and Nathan D. Webb

Illinois State Geological Survey, Prairie Research Institute, University of Illinois at Urbana-Champaign

Circular 602 2020

ILLINOIS STATE GEOLOGICAL SURVEY
Prairie Research Institute
University of Illinois at Urbana-Champaign
615 E. Peabody Drive
Champaign, Illinois 61820-6918
http://www.isgs.illinois.edu

ILLINOIS
Illinois State Geological Survey
PRAIRIE RESEARCH INSTITUTE

Suggested citation:
Grigsby, N.P., and N.D. Webb, 2020, Assessing the Cypress Sandstone for carbon dioxide-enhanced oil recovery and carbon storage: Part II—Leveraging geologic characterization to develop a representative geocellular model for Noble Oil Field, western Richland County, Illinois: Illinois State Geological Survey, Circular 602, 19 p.

Contents

Tables

Figures

ABSTRACT

This research aims to leverage the geologic characterization by Webb and Grigsby (2020) to develop a geocellular model that represents the static reservoir properties (porosity and permeability) of the Cypress Sandstone at Noble Field in Richland County, Illinois. This model will be used to create hypothetical carbon dioxide-enhanced oil recovery (CO_2-EOR) injection simulations to determine whether, and under what conditions, the reservoir and its underlying residual oil zone (ROZ) could add to incremental oil production at the field. Geologic characterization played a key role in model development. It was necessary to clearly delineate the contact between the thick fluvial sandstone interval and the overlying shaley estuarine interval so that a geostatistical analysis could isolate and detect the anisotropy and transitional behavior within each element. In addition, this new understanding of the sedimentology and depositional environment provided context for inferring interwell characteristics or small-scale features that could have a substantial impact on fluid flow without producing a strong signal on geophysical logs.

A large number of spontaneous potential (SP) logs were collected at Noble Field, which were used to detect a strong northwest–southeast-trending anisotropy and condition simulations to model the distribution of sandstone and shale. From detailed evaluation of whole core and neutron-density porosity logs, two thin (1.5 to 3 ft thick, or 0.5 to 1 m thick) layers of low-porosity calcite cement were found, which were not observed on the SP logs. These cement layers were interpreted to have formed at the oil–water contact and to act as laterally continuous baffles to vertical fluid flow. Data from neutron-density porosity logs were used to detect the calcite-cemented layers and incorporate them into the model. Too few of these logs were available to characterize the field-wide lateral anisotropy in sandstone and shale, but geostatistical analysis of the porosity logs did indicate two parallel layers of calcite cement, one at the oil–water contact and one about 9 ft (3.3 m) below it. Combining the model based on the SP logs and the model based on the neutron-density porosity logs resulted in a model that properly represented the distribution of depositional (sandstone and shale) and digenetic (calcite cement) geologic features that control fluid flow.

INTRODUCTION

Noble Oil Field is located in secs. 3, 4, 5, 8, 9, 17, and 18, T3N, R9E, and secs. 32 and 33, T4N, R9E, in Richland County, Illinois. Although oil production in the field is commingled from several formations, about half of the oil produced from the field, or approximately 24 million barrels of oil (MMBO), has been produced from the valley-fill Cypress Sandstone (Webb and Grigsby 2020). Detailed reservoir characterization of the Cypress has identified a substantial amount of unswept oil (75% of original oil in place [OOIP]) remaining in the conventional reservoir and the potential for a thick zone (>100 ft, or 30.5 m) of relatively low oil saturation and high water saturation, known as a residual oil zone (ROZ; Webb and Grigsby 2020). Carbon dioxide-enhanced oil recovery (CO_2-EOR) may be particularly useful in reservoirs that contain a thick ROZ beneath a main pay zone for two reasons: (1) CO_2-EOR has been shown to effectively produce residual oil bypassed by anthropogenic or natural waterflooding (Blunt et al. 1993; Hill et al. 2013), and (2) the thick ROZ has the capacity to store a significant amount of CO_2. Therefore, even though the field has already been developed and has undergone primary recovery and secondary waterflooding, CO_2-EOR could be used to extract the residual oil remaining in both the ROZ and the main pay zone and store large volumes of CO_2.

Reservoir simulations of hypothetical CO_2 injection scenarios are a convenient and inexpensive way of addressing technical and operational questions and minimizing the risk associated with nonconventional CO_2-EOR projects (Kovscek and Cakici 2005). The heterogeneity and anisotropy of porosity and permeability strongly influence fluid flow, so reservoir simulations rely on a geocellular model that accurately represents the geologic architecture of the reservoir. Geocellular models are typically built on conditioning data from well logs, but because many oil fields throughout the Illinois Basin were developed in the first half of the 20th century, they commonly lack the data coverage obtained from modern well logs (such as neutron-density porosity) that are typically used in model construction. Therefore, it is often necessary to incorporate information from the abundance of old logs (such as spontaneous potential [SP] or resistivity) that do not directly indicate porosity or permeability.

This research aims to leverage the geologic characterization by Webb and Grigsby (2020) to develop a geocellular model that represents the static reservoir properties (porosity and permeability) of the Cypress Sandstone at Noble Field. This model will be used to create hypothetical CO_2-EOR injection simulations to determine whether, and under what conditions, the ROZ could add to incremental oil production at the field.

GEOLOGIC CHARACTERIZATION

Webb and Grigsby (2020) conducted a reservoir characterization of the valley-fill Cypress Sandstone in Noble Field, and the reader is referred to that report for details on the geology, historical oil production, and fluid properties of the oil reservoir. This characterization revealed that the Cypress is composed of multistory fluvial sandstone deposited during lowstand and transgression, with evidence of a change to estuarine conditions near the top. Geophysical logs indicated a relatively homogenous sandstone, but careful examination showed some internal compartmentalization in the form of laterally continuous shale breaks near the top and base and thin calcite-cemented zones in the upper reservoir concurrent with the oil–water contact. The sandstone is of high reservoir quality, with high porosity and permeability (Table 1). The upper portion of the reservoir transitions from a clean fluvial sandstone to a shale-rich estuarine interval.

Geologic characterization played a key role in model development. It was necessary to clearly delineate the contact between the thick fluvial sandstone interval and the overlying shaley estuarine interval so that a geostatistical analysis could isolate and detect the anisotropy and transitional behavior within each element. In addition, this new understanding of the sedimentology and depositional environment provided context for inferring interwell characteristics or small-scale features that could have a

Table 1 Summary of core analysis data and statistics from Noble Field[1]

Petrophysical property	Minimum (P10)	Maximum (P90)	Median	Mean	Standard error
Porosity, %	13.5	20.3	17.4	17.0	0.18
Permeability, mD (μm^2)	10.0 (0.01)	960.8 (0.95)	365.0 (0.36)	438.7 (0.43)	25.6

[1]From Webb and Grigsby (2020).

substantial impact on fluid flow without producing a strong signal on geophysical logs.

METHODS

Data

In total, 385 SP logs and 126 neutron-density porosity logs from 386 wells within Noble Field were used to develop the geocellular model (Figure 1). Core analysis reports for the thick Cypress Sandstone from 14 wells within Noble Field and 13 wells from the thick Cypress Sandstone elsewhere in Richland County were also used (Table 1). Both the log and core data are available from ILOIL, a database of well information on the Illinois State Geological Survey website (https://www.isgs.illinois.edu/illinois-oil-and-gas-resources-interactive-map).

Enough wells with SP logs were available for Noble Field to clearly delineate lithofacies boundaries and detect large-scale anisotropy within the sandstone. However, two layers of calcite cement observed in core were either ionically permeable or too thin to be detected by SP logs. Conversely, an insufficient number of wells with porosity logs were available to quantify large-scale trends in sandstone and shale, although the logs did detect two parallel layers of calcite cement observed in the core and sample sets (Figure 2). Thus, the strengths of both data types were leveraged to capture different aspects of the geologic heterogeneity within the Cypress Sandstone: SP logs were used to develop a model of the depositional distribution of lithofacies (i.e., sandstone and shale; hereafter referred to as the "depositional model"), and porosity logs were used to develop a model of the diagenetic calcite cement within the sandstone (hereafter referred to as the "diagenetic model"). The two models were combined to create a geocellular model representative of the internal architecture of the Cypress Sandstone at Noble Field that included depositional and diagenetic geologic features believed to control the fluid flow.

Grid Development

Both models were based on a three-dimensional grid constructed to encompass the lateral extent of the study area, covering ~666 million ft^2 (~24 mi^2, or 62 km^2; Figure 1) and a volume of ~250 billion ft^3 (7 million m^3). The grid was divided into ~25 million cells (260 × 256 × 375) with cell dimensions of $\Delta x = \Delta y = 100$ ft (30.5 m) and $\Delta z = 1$ ft (0.3 m).

Structure maps of the base of the Beech Creek ("Barlow") Limestone and the base of the thick Cypress Sandstone developed during geologic characterization provided boundaries for the vertical extent of the grid. An additional structure map of the top of the thick Cypress Sandstone was used to demarcate a gross lithofacies change from the lower, reservoir-quality sandstone portion of the Cypress Sandstone (referred to here as the "thick Cypress") to the upper, non-reservoir-quality shale-rich zone (referred to here as the "upper Cypress"; Figure 3).

Depositional Model Development

Spontaneous potential logs had the highest data density and were used to quantify the lithofacies distribution. The SP logs for each well were normalized to compensate for the well-to-well variation that occurs because of differences in fluid chemistry or other borehole conditions (Leetaru 1990). Webb and Grigsby (2020) described the process of normalizing SP logs in detail. Normalizing involved selecting consistent deflection points for the sandstone and shale and rescaling the curves to set these points as 100 and 0, respectively. The Fraileys Shale was used for the shale baseline, and the thick Cypress Sandstone was used as the sandstone baseline. The normalized curve was considered analogous to the proportion of sandstone versus shale.

The base of the Beech Creek Limestone was used as a stratigraphic datum to convert the grid and log data from structural space to stratigraphic space. Doing so aligned features such as shale beds and equivalent sandstone facies that were assumed to have been deposited on a horizontal plane. This alignment was necessary for the variograms to detect anisotropy and spatial correlations.

The normalized SP logs were used to develop variogram maps to detect the direction of anisotropy. The resulting variogram map of the thick Cypress showed clear anisotropy, with maximum connectivity in the N110° direction (Figure 4). This result matched the dominant northwest–southeast-oriented thick sandstone body mapped by Webb and Grigsby (2020; Figure 5). No clear anisotropy could be detected for the shale-rich zone above the thick Cypress because it did not contain a substantial number of discreet sandstone bodies within the model domain.

The spatial correlations of the thick Cypress Sandstone were quantified by using two empirical horizontal variograms: one aligned with the direction of maximum connectivity (N110°) and one perpendicular to it (N200°). One empirical vertical variogram was also used.

Models fit to each variogram had two nested structures: one with short ranges that controlled the data assigned to cells close to the conditioning data, and one with much longer ranges that controlled the data assigned to cells far from the conditioning data (Figure 6). Each structure had the same sill (the proportion of variance assigned to each structure) and a small nugget (variance allowed from measured data) to honor the conditioning data. The model aligned with the direction of maximum connectivity had much longer ranges (Table 2), which resulted in features within the model elongating in that direction. Because no anisotropy could be detected in the upper

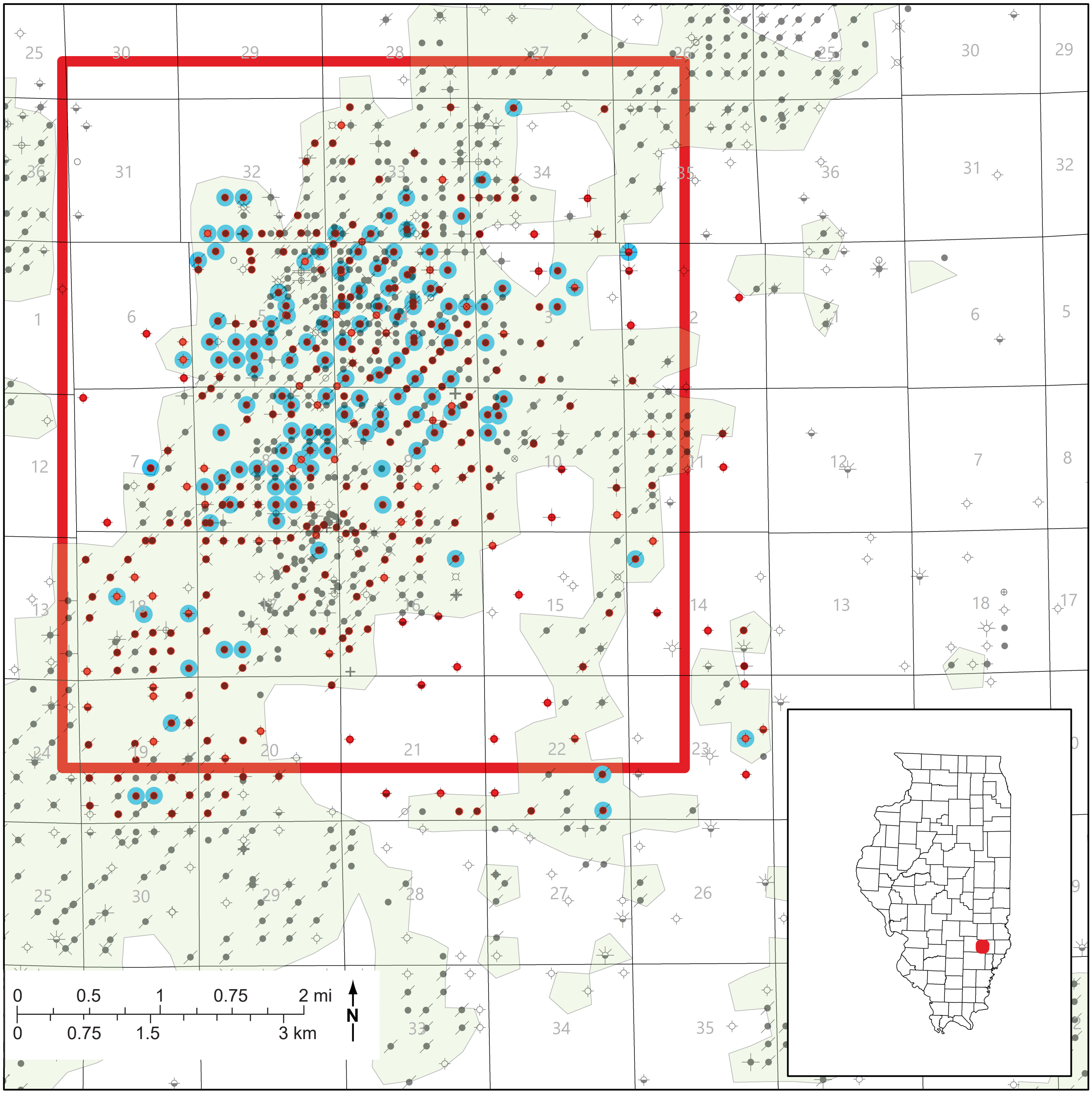

Figure 1 Map of Noble Field showing the model extent (red box) and data distribution. The small red dots indicate wells with spontaneous potential logs, and the large blue dots indicate wells with neutron-density logs.

Cypress, an omnidirectional variogram was used.

The variogram models were used in sequential Gaussian simulations to create 50 unique, equiprobable realizations of the distribution of normalized SP values for both the thick Cypress and the upper shale-rich zone. The realizations were compared with the geologic characterization of Webb and Grigsby (2020), and Illinois State Geological Survey geologists assisted in choosing the realization that best represented the internal architecture and heterogeneity.

Diagenetic Model Development

In total, 126 neutron-density porosity logs were used to create a diagenetic model of the calcite cement and unaltered sandstone. Because the calcite cement is a diagenetic feature believed to have been formed at the oil–water contact (Webb

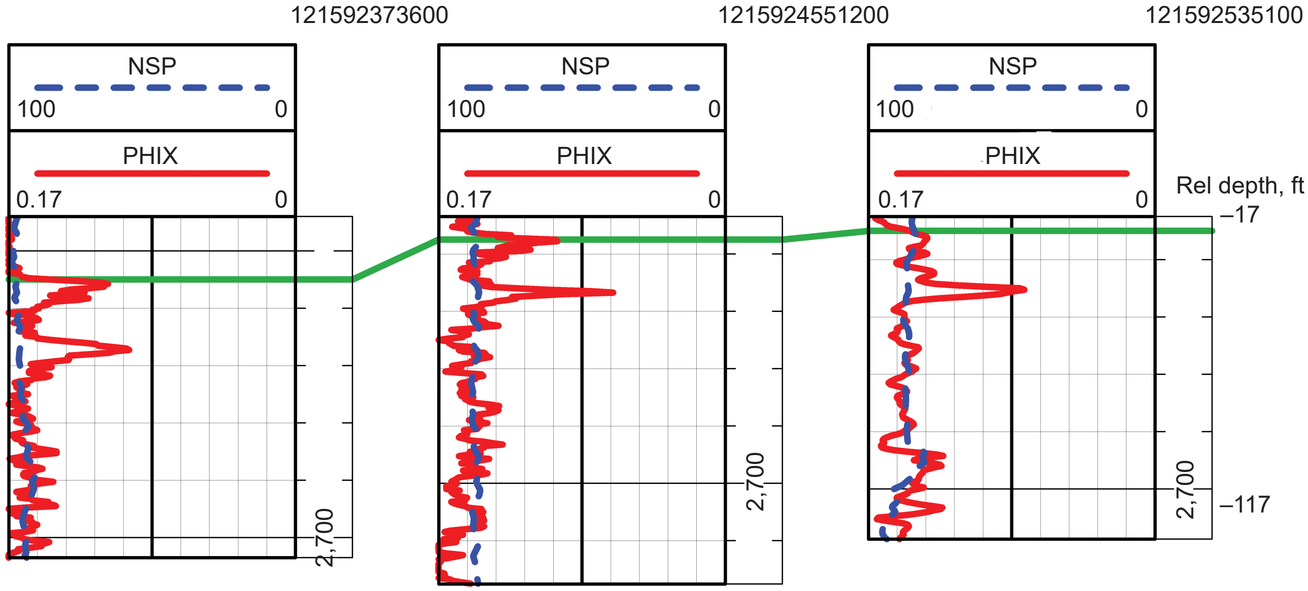

Figure 2 Digitized log data for the thick Cypress from three wells within Noble Field. The red lines indicate cross-plotted porosity (PHIX) values, and the blue lines indicate normalized spontaneous potential (NSP) values. The green line is the interpreted oil–water contact. The NSP had less variability but was able to approximate the porosity log, except for two calcite cement layers that occurred at the oil–water contact and approximately 9 ft (3.3 m) below it.

and Grigsby 2020), the grid and log data were flattened along the oil–water contact instead of at the base of the Beech Creek Limestone. This shifted the data to the orientation at which the geologic feature was believed to have been created.

A porosity cutoff of 15% was used to separate the logged data into cement (<15%) and unaltered sandstone facies (>15%; Figure 7). From core data, the calcite cement was known to have a porosity of approximately 10%, but the cement layers were not always thick enough for neutron-density porosity logs to record the true porosity. However, because the unaltered sandstone was relatively homogenous and typically had a porosity of 16% to 18%, values below what were observed for sandstone were attributed to cement.

Geostatistical analysis of the neutron-density logs detected two parallel layers of calcite cement, one at the oil–water contact and one approximately 9 ft (3.3 m) below it. Of the 126 wells with neutron-density porosity logs, both layers of calcite cement were present in 97 wells, and 12 wells had only the deeper layer of calcite cement (Figure 7). The cement was not detected by logs in the remaining 17 wells. The calcite cement was most prevalent in the middle of the model and absent in the northeast. Low-porosity "cement" facies also occurred sporadically near the base of the model, as was noted by Webb and Grigsby (2020).

The grid was divided into three zones: one with wells with two cement layers, one with wells with one cement layer, and one with wells without a cement layer. The odds of encountering the cement facies were calculated for each layer within each zone. Trends were interpolated between zones, and each cell was assigned the odds of encountering the cement facies. This method extrapolated trends over the entire grid and was not good at detecting lateral variability, but it was appropriate for recreating the calcite cement, which was interpreted to be laterally continuous.

Assignment of Petrophysical Properties

The depositional and diagenetic models were returned to structural space and combined to create a model that incorporated the geologic heterogeneity, including the lithofacies distribution and diagenetic calcite cement.

Porosity values were assigned to each cell by developing a transform based on wells that had both SP and neutron-density porosity logs. The data were plotted against each other and a line was regressed through them. Ideally, the equation defining this regression line would have been used to transform the normalized SP values in each cell into porosity (Figure 8a). However, the logs were known to include the calcite cement facies that appeared as clean sandstone on the SP logs but that had low porosity on the porosity logs. Thus, to create a transform for the unaltered sandstone, an attempt was made to identify data from the calcite-cemented intervals. The SP and porosity curves for each well were analyzed, and data points that fell within cement zones were identified (Figure 8b). The points that fell within the cement zones generally had high SP and low porosity values. These points were removed, and a new line was regressed through the remaining data (Figure 8c). The transform based only on clean sandstone data points resulted in modeled porosity that was closer to core values (Table 3), so it was used to transform the simulated normalized SP values in each cell into porosity.

The diagenetic model was returned to structural space, and cells that had a high probability of containing the low-porosity

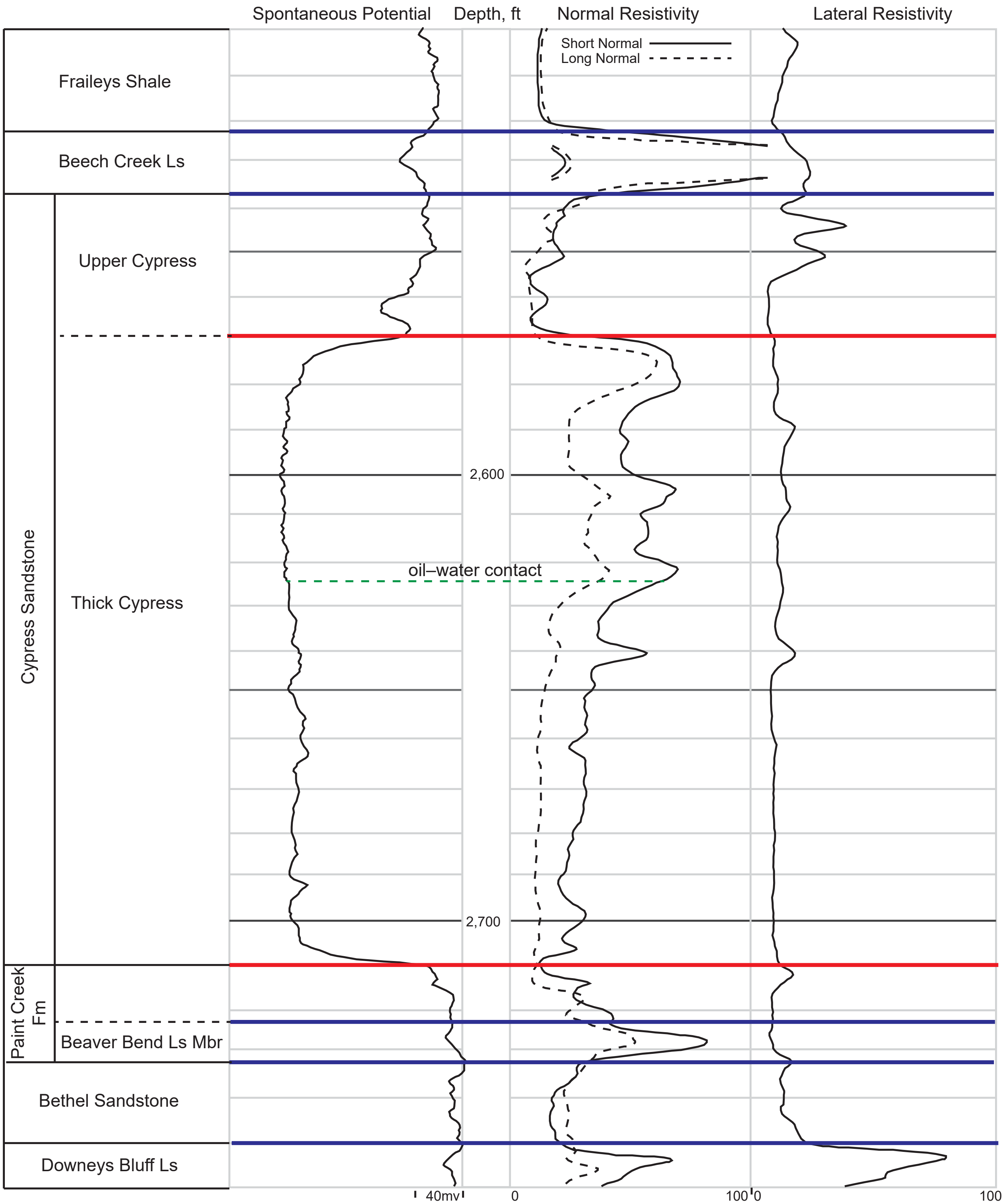

Figure 3 Type electric log of the valley-fill Cypress Sandstone in Noble Field from the C.T. Montgomery B-15 well (API 121590140400, SW¼NW¼ sec. 4, T3N, R9E). The "thick Cypress" Sandstone consists of approximately 140 ft (42.7 m) of sandstone overlain by approximately 35 ft (10.7 m) of "upper Cypress" shale and shaley sandstone. Roughly 53 ft (16.2 m) of oil reservoir is developed in the top of the sandstone, as indicated by the resistivity profile and confirmed by the sample descriptions on file at the ISGS. Modified from Webb and Grigsby (2020).

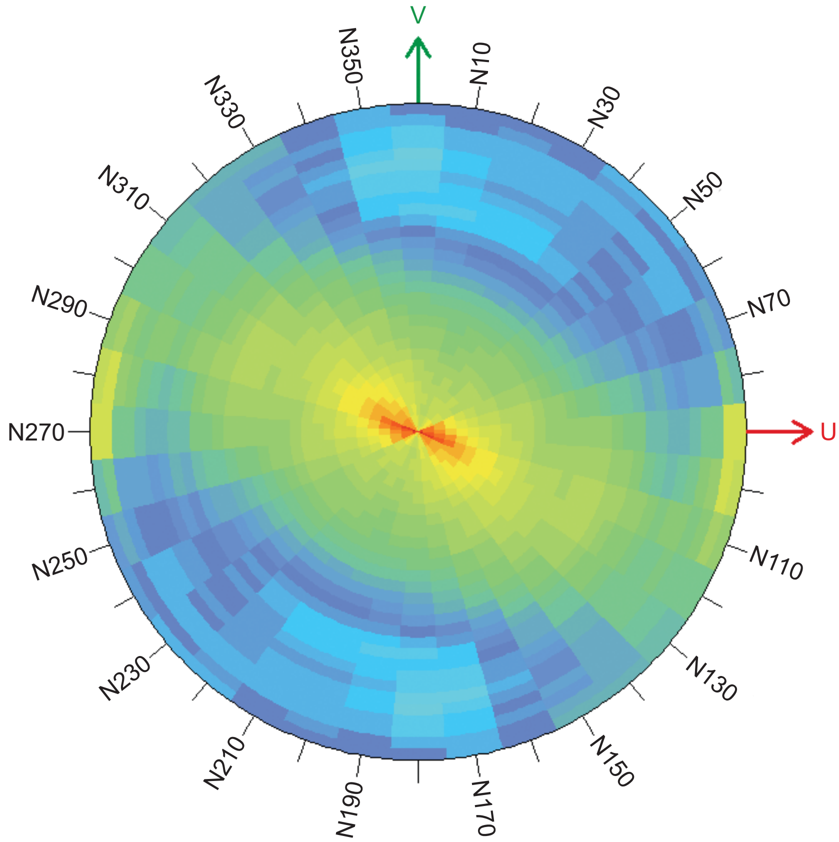

Figure 4 Visual representation of the spatial correlations in every compass direction. Warm colors indicate normalized spontaneous potential values that were similar to the point of origin. Warm colors aligning along N110° indicate a long range of spatial correlation along that direction, which aligns with the predominantly northwest–southeast trend of the Cypress Sandstone (Webb and Grigsby 2020). Conversely, cool colors perpendicular to N110° indicate that values became different near the point of origin and had a short range of spatial correlation in that direction. V, north; U, east.

facies (>90%) were embedded in the depositional model. These cells were then assigned a porosity of 10%.

A porosity-to-permeability transform was developed by using data from conventional core plug analysis reports for the Cypress Sandstone at Noble Field available on ILOIL (https://www.isgs.illinois.edu/illinois-oil-and-gas-resources-interactive-map). A crossplot of the raw data appeared to contain two trends, one with high permeability and one with lower permeability (Figure 9a). The existence of two separate trends suggested that two porosity-to-permeability relationships existed within the Cypress Sandstone, most likely related to changes in facies within the sandstone (Webb and Grigsby 2020).

The upper shaley estuarine portion of the sandstone was expected to have lower porosity and permeability values than were samples in the cleaner fluvial sandstone because of the abundance of lower energy bedforms and the higher clay content (Webb and Grigsby 2020). The depth of each data point was subtracted from the depth to the top of the thick Cypress for each well. The results were sorted into three groups: one containing data from the upper Cypress, one with data from less than 10 ft (3 m) below the top of the thick Cypress (near the contact of the thick and upper Cypress), and one with data from the middle of the thick Cypress.

Data from the middle of the thick Cypress, where higher energy cross-bedded sandstones with very little clay content are dominant, generally fell within the higher permeability trend, whereas data from the upper Cypress fell within the lower permeability trend (Table 4). Two reduced major axis lines were created for each trend, one fit to the data from the heterolithic estuarine upper Cypress, and the other fit to the data from the more homogeneous, fluvial middle of the thick Cypress. Data that fell within 10 ft (3 m) below the top of the thick Cypress fell into both trends and were not included in either regression (Figure 9b). Averaging the data for each core reduced scatter and made both trends more distinct (Figure 9c).

The equation defining the line fit to the data from the thick Cypress (green line in Figure 9b and 9c) was used to transform

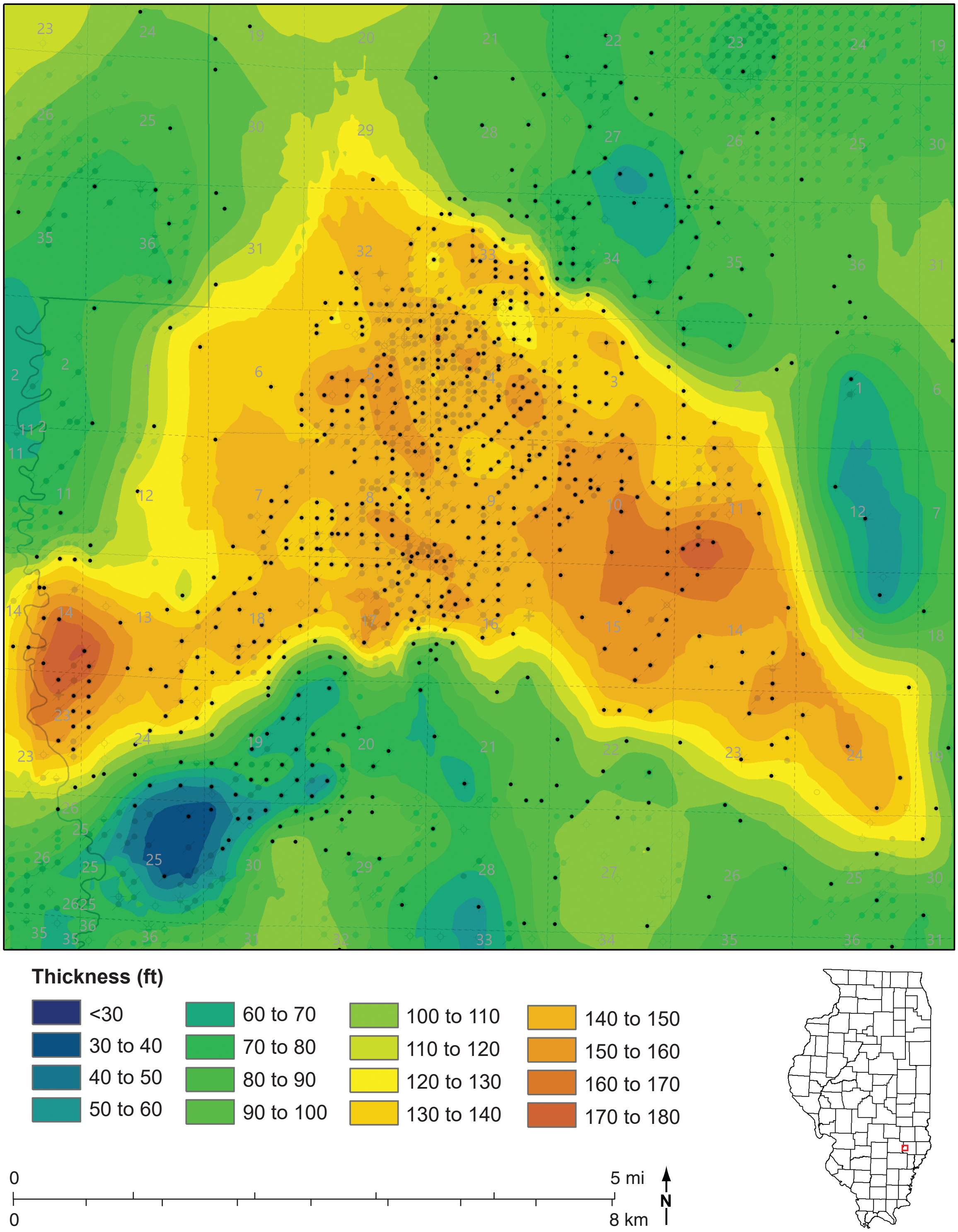

Figure 5 Isopach map of Noble Field showing the valley-fill Cypress Sandstone. The contour interval is 10 ft (3.0 m). The map shows an intersecting northwest–southeast and northeast–southwest trend of maximum thickness, which is oblique to the northeast–southwest trend of the overall valley-fill Cypress Sandstone fairway. Data points are shown on the map as black dots. Reprinted from Webb and Grigsby (2020).

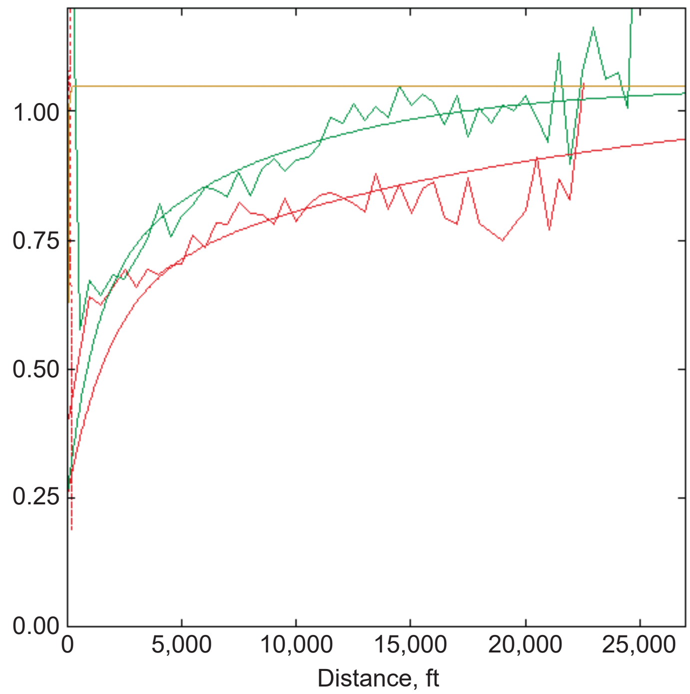

Figure 6 Models fit to the horizontal variograms for the thick Cypress, including the one in the direction of maximum connectivity (N110°, red lines) and the one perpendicular to it (N200°, green lines). The model variograms (smooth lines) fit the empirical variograms (choppy lines), indicating that transitional behavior was captured. The *y*-axis shows semi-variance.

Table 2 Statistics for the horizontal variograms aligned with the anisotropy (N110°) and perpendicular to it (N200°), and for the vertical variogram (*z*)[1]

Direction	Nugget	Close sill	Close range, ft (m)	Far sill	Far range, ft (m)
N110°	0.1	0.5	5,500 (1,676)	0.4	60,000 (18,288)
N200°	0.1	0.5	3,500 (1,067)	0.4	25,000 (7,620)
z	0.1	0.5	40 (12)	0.4	120 (36.6)

[1]The sill represents the variance assigned to each structure and the nugget represents measurement errors (how far the model was allowed to deviate from the conditioning data).

the porosity into permeability in the model of the thick Cypress, and the equation defining the line fit to the data from the upper Cypress (blue line in Figure 9b and 9c) was used to transform porosity to permeability in the model of the upper Cypress. These transforms resulted in higher permeability values for the model of the thick Cypress (Table 4) that were believed to be a better approximation of the cross-bedded sandstone and lower values for the model of the upper Cypress that were believed to be a better approximation of the upper shaly interval.

RESULTS AND DISCUSSION

Depositional Model Results

The modeled distribution of sandstone and shale matched expectations from the geologic characterization. The thick Cypress is primarily composed of sandstone with a low clay content (Table 5), and isolated shale breaks transition into shale at the top (Figures 10 and 11). The character of the model began to change to the northeast as the thick Cypress thinned and became slightly more shaley, corresponding to the transition into Noble North Field. In addition, the large-scale anisotropy observed along N110° in the variogram map coincided with the elongation of the thickness of the sandstone body observed on the isopach map (Figure 5).

The model of the upper Cypress was much more shale rich than was the lower thick sandstone, in which northeast–southwest-trending sandstone lenses occurred only in the northeast corner (Figure 12). This result coincides with an overall thinning of the thick Cypress and the development of discrete sandstone

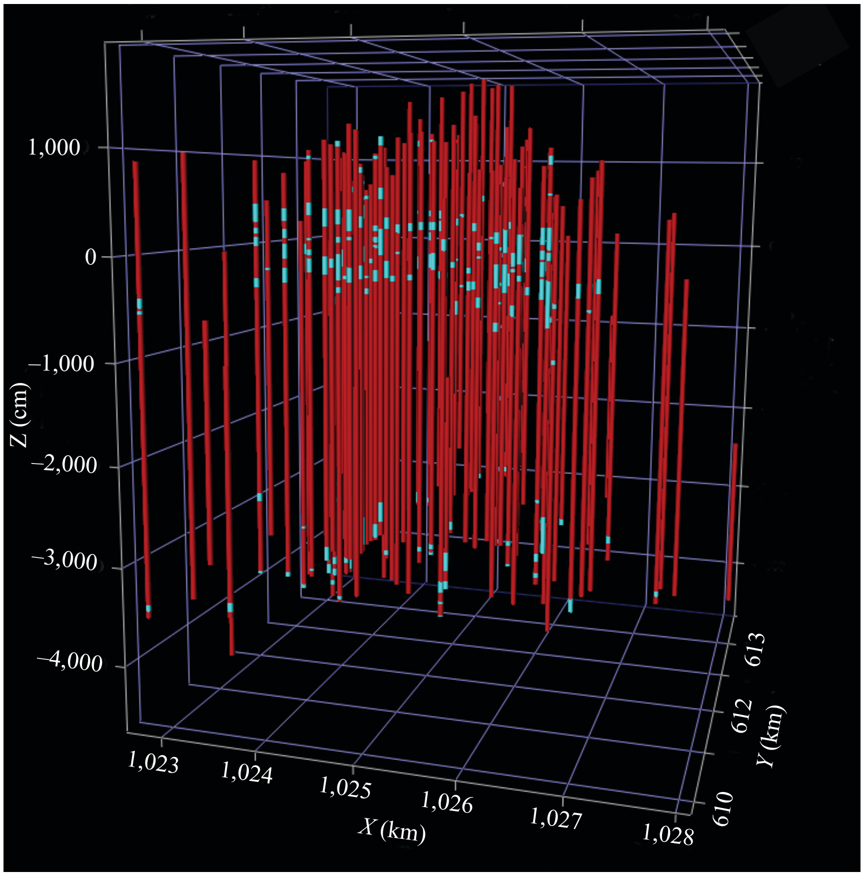

Figure 7 Distribution of high-porosity (unaltered) facies in red and low-porosity (calcite cement) facies in blue used for the diagenetic model. The data were flattened along the oil–water contact. Most of the low-porosity facies occurred in two bands near the top and sporadically near the base.

lenses in the shale-rich upper Cypress in Noble North Field. The upper Cypress will not be used for reservoir simulations because it is not hydraulically connected to the main thick Cypress sandstone body. However, the fact that the model matched expectations from the geologic conceptual model of Webb and Grigsby (2020) demonstrates that (1) the SP logs were able to detect changes in lithofacies and (2) the data coverage was adequate to detect anisotropy and to condition simulations to create a representative distribution. Both findings improved confidence in the depositional model of the thick Cypress.

Diagenetic Model Results

The diagenetic model had two parallel layers of cement: one concurrent with the existing oil–water contact and the other approximately 9 ft (3.3 m) below it (Figures 13 and 14). The lower layer was often more pronounced, but both layers were present throughout the model, except in the northeast corner, where the cement thinned and disappeared. This result corresponds to the transition to Noble North Field, where the upper thick Cypress becomes more shale rich and the top of the sandstone dips below the plane of the cement.

The diagenetic model had low porosity near the base of the thick Cypress. These data points were interpreted as discontinuous shale units that appeared as clean sandstone transitions to shale at the base of the reservoir. The depositional model properly represented these discontinuous shale bodies, and the odds of encountering these layers in the diagenetic model were below the threshold used to embed cement in the final model. Thus, the layers were not included in the final model.

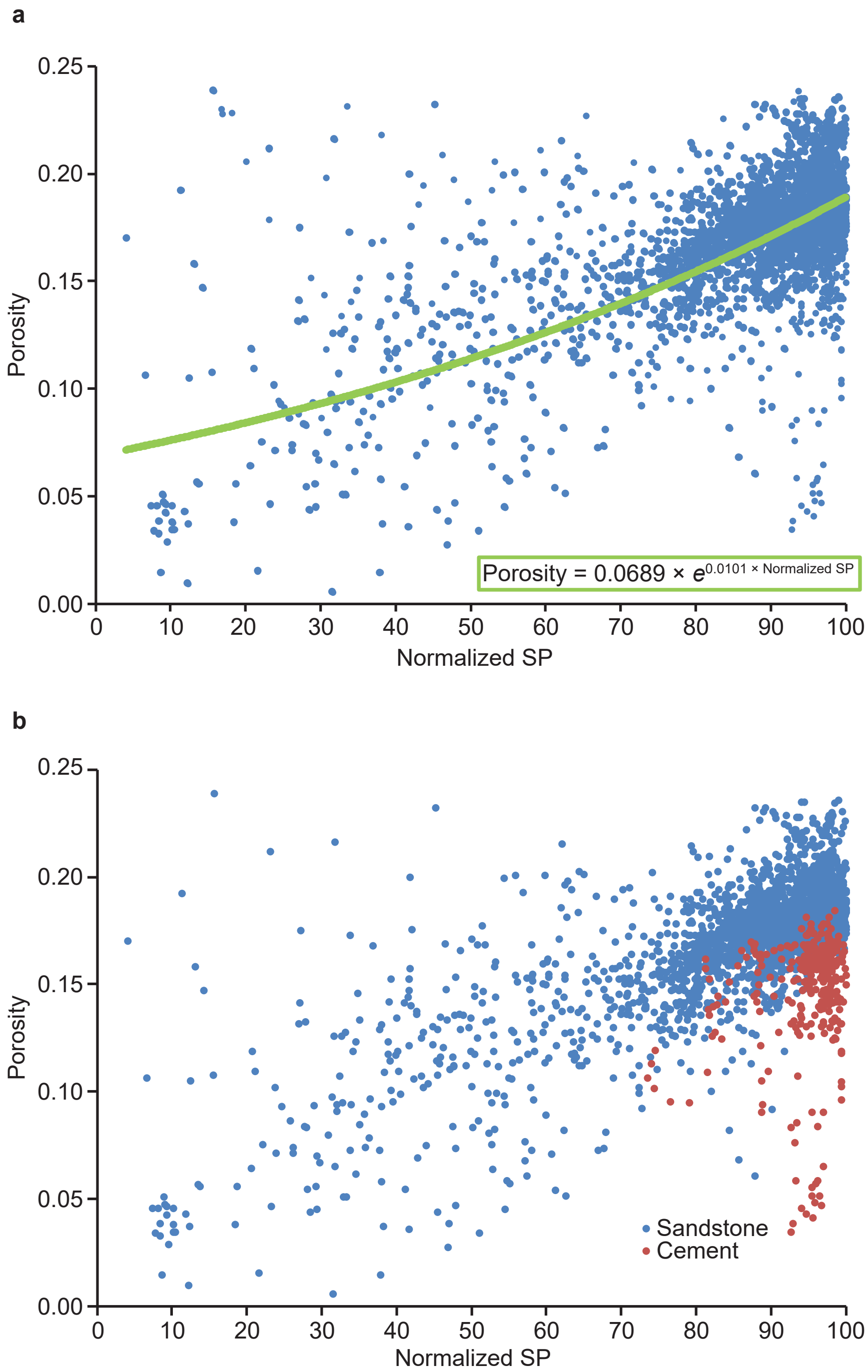

Figure 8 Crossplots of the normalized spontaneous potential (SP) and neutron-density porosity values, including raw data (a), grouped by clean sandstone and cement facies (b) and clean sandstone only (c, p. 11). The reduced major axis lines were fit to raw data (green line) and to clean sandstone only (red line). The equation defining the red line was used to transform simulated normalized SP values into porosity. Porosity is displaced as a decimal fraction, and normalized SP is analogous to the percentage of clean sandstone.

c

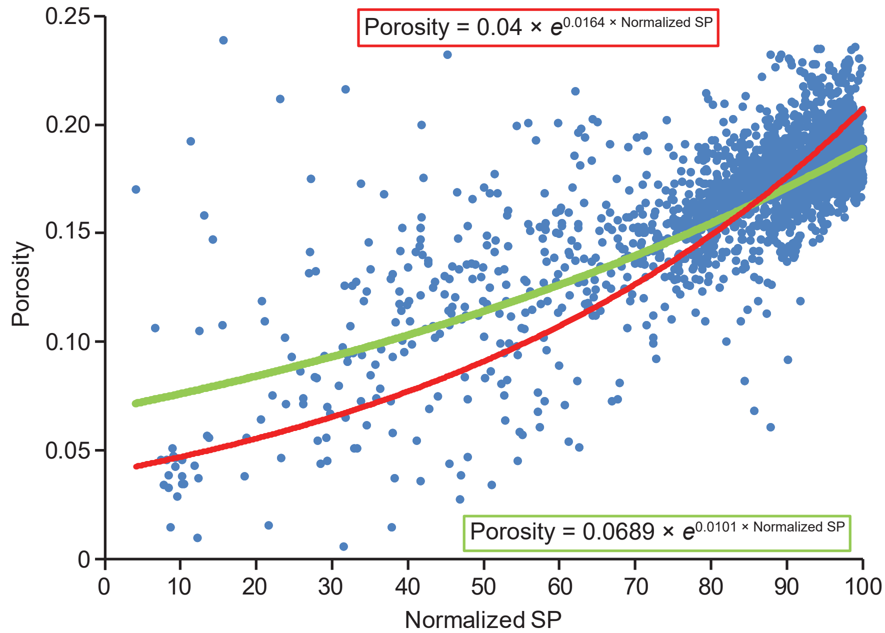

Figure 8 *Continued.*

Table 3 Porosity from core analysis reports and derived from spontaneous potential logs by using transforms based on all data and clean sandstone only

		Model porosity, %	
Statistic	Core porosity, %	All data transform	Clean sandstone only transform
Minimum	6	8	5
Maximum	25	18	21
Mean	17	17	17
Median	18	17	18

a

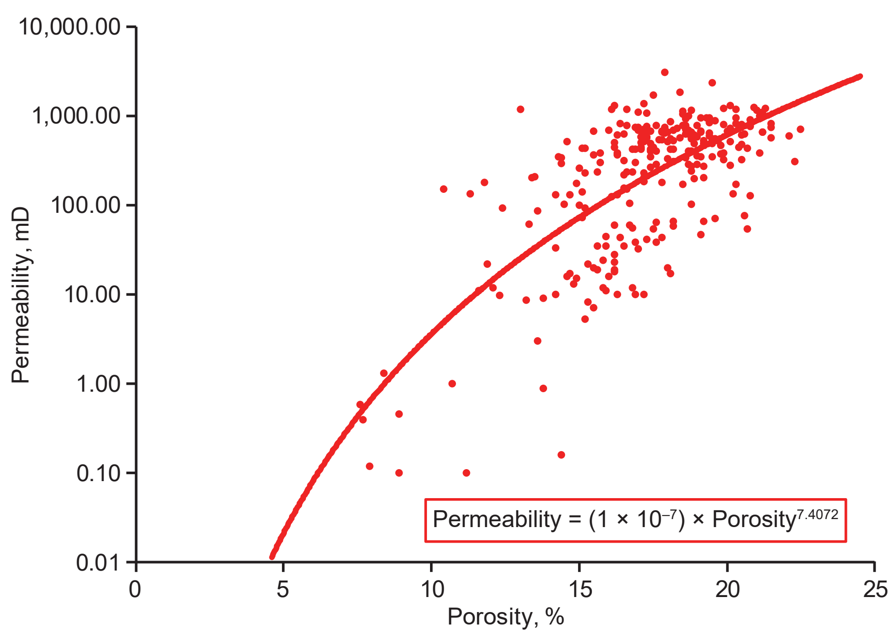

Figure 9 Crossplot of porosity and permeability from core analysis reports. The raw data (a) contained two trends, so the data were grouped by depth above or below the top of the thick Cypress (b, p. 12). This process revealed that the data from the upper Cypress occurred in a lower permeability cluster, whereas data from within the thick Cypress generally occurred in a higher permeability cluster. This behavior became even more apparent when the data were averaged for each core (c, p. 12).

b

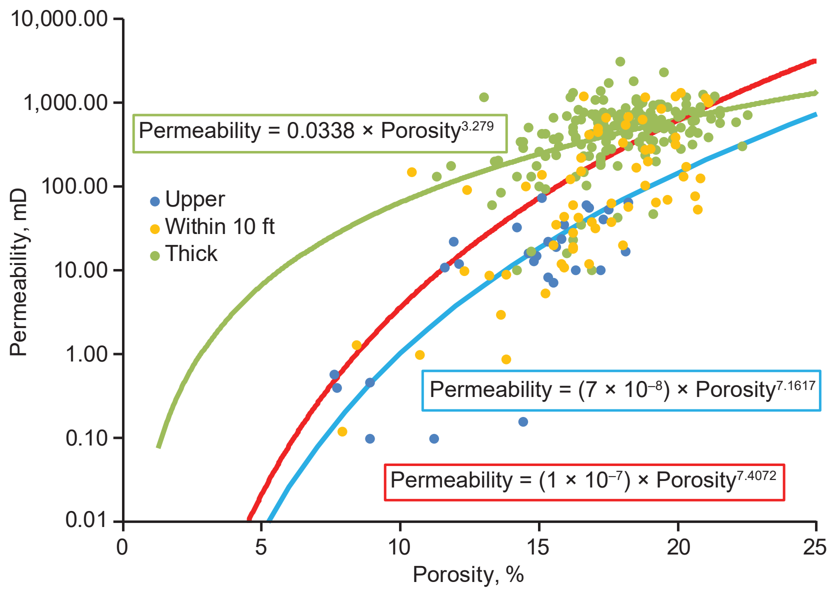

c

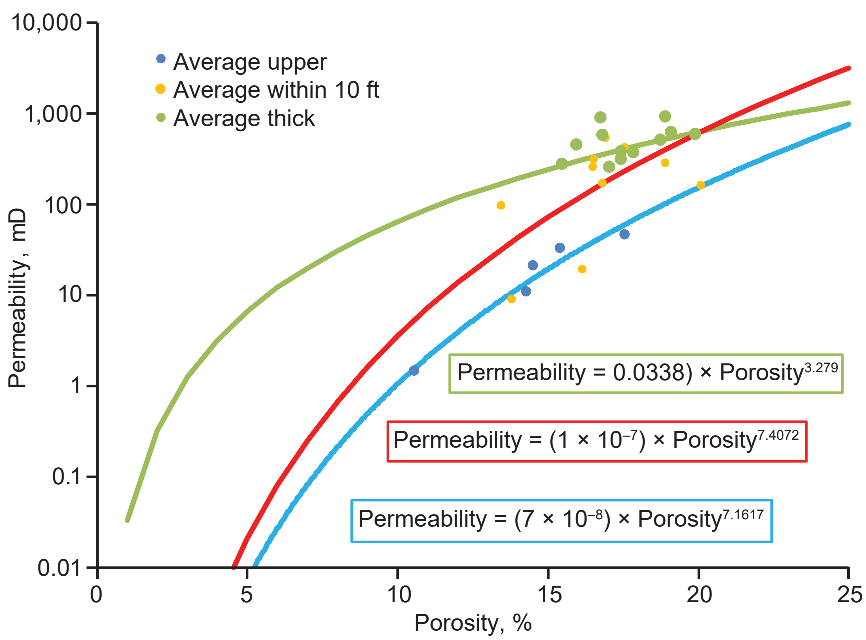

Figure 9 *Continued.*

Table 4 Permeability statistics from core analysis reports and derived from porosity for the model by using two transforms

Statistic	Core, mD (μm²)	Combined transform, mD (μm²)	Thick only transform, mD (μm²)
Minimum	0.10 (0.00)	0.00 (0.00)	3.07 (0.00)
Maximum	6,170.00 (6.09)	543.63 (0.54)	689.47 (0.68)
Mean	562.85 (0.56)	215.07 (0.21)	409.12 (0.40)
Median	342.00 (0.34)	222.25 (0.22)	461.24 (0.46)

Table 5 Percentage of clean sandstone in the thick Cypress and in the shale-rich upper Cypress[1]

Statistic	Upper Cypress, % clean sandstone	Thick Cypress, % clean sandstone
Minimum	0	0
Maximum	100.00	100.00
Mean	13.75	88.20
Median	8.87	93.57
Standard deviation	14.67	15.03

[1]Normalized spontaneous potential values were considered analogous to the percentage of clean sandstone. The thick reservoir portion contained much cleaner sandstone, whereas the upper shale rich zone had a very low sandstone content.

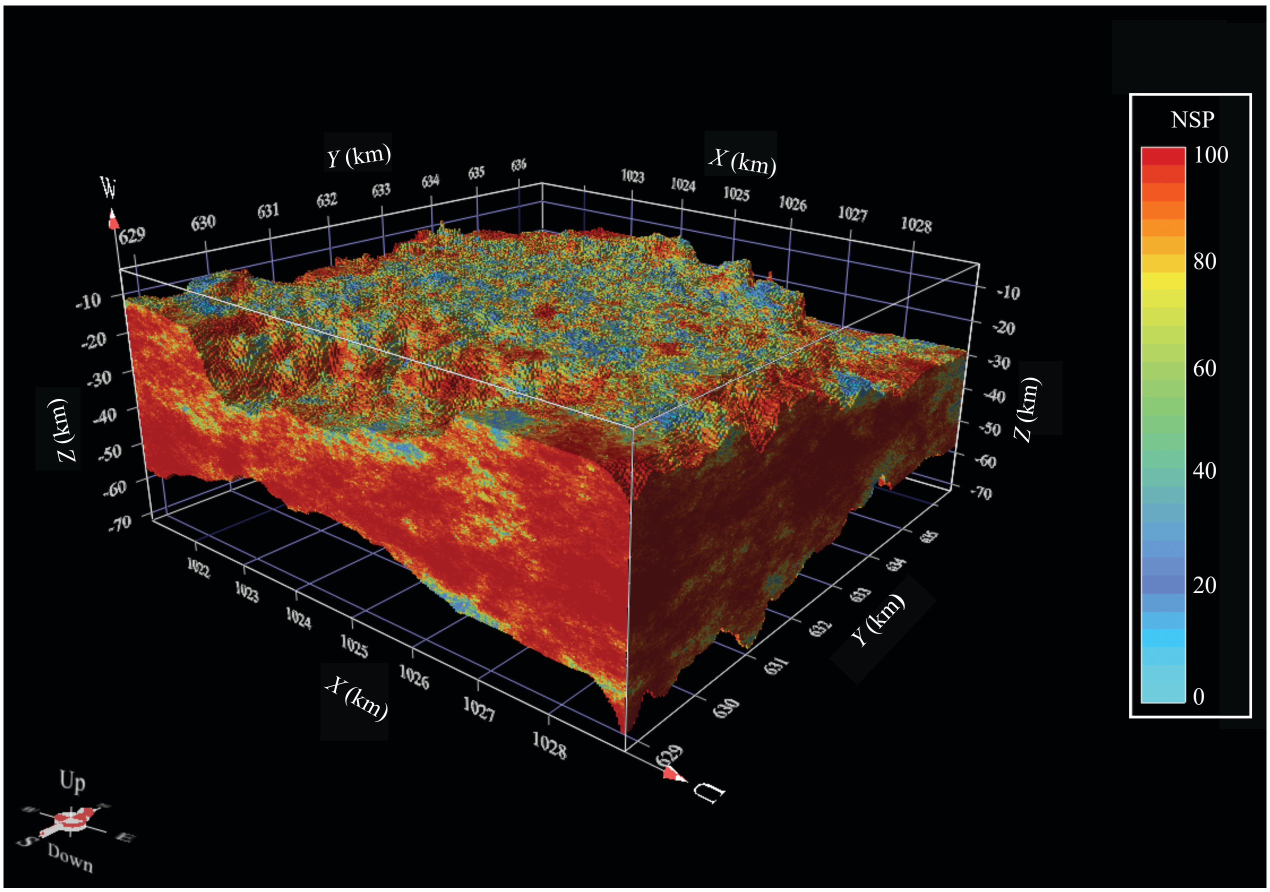

Figure 10 Distribution of the normalized spontaneous potential (NSP) values in the depositional model. Warm colors indicate cells with a high percentage of sandstone, and cool colors indicate cells with a high percentage of shale. The middle of the model is very sandstone rich, and the upper and lower bounds are much more shale rich than the middle of the model. The model is shown in stratigraphic space with a 50× vertical exaggeration. W, up; U, east.

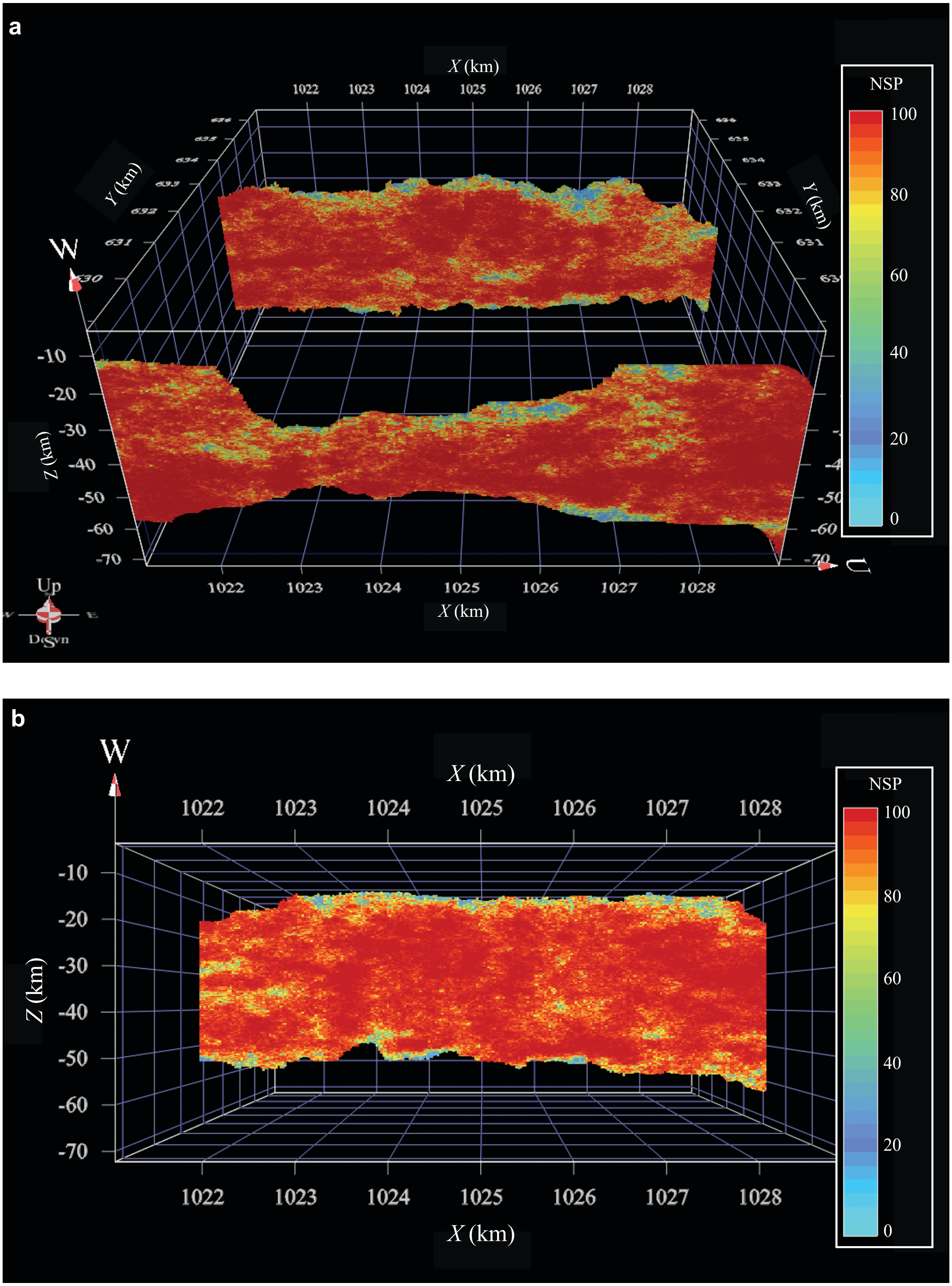

Figure 11 East–west slices of the depositional model showing the internal distribution of sandstone and shale. The slices in the upper image represent the distribution at the southern and northern borders. (The northern border is ~16,000 ft [4,877 m] from the southern border.) The slice in the lower image represents the middle of the model and is ~10,000 ft (3,048 m) from the southern border. All slices reveal that the middle of the model is mostly clean sandstone with a few discontinuous shale units and that the most pronounced shale appears at the upper and lower boundaries. The northernmost slice has more shale in the eastern corner, coinciding with the transition to Noble North Field. All slices are shown in stratigraphic space with a 50× vertical exaggeration. NSP, normalized spontaneous potential; W, up; U, east.

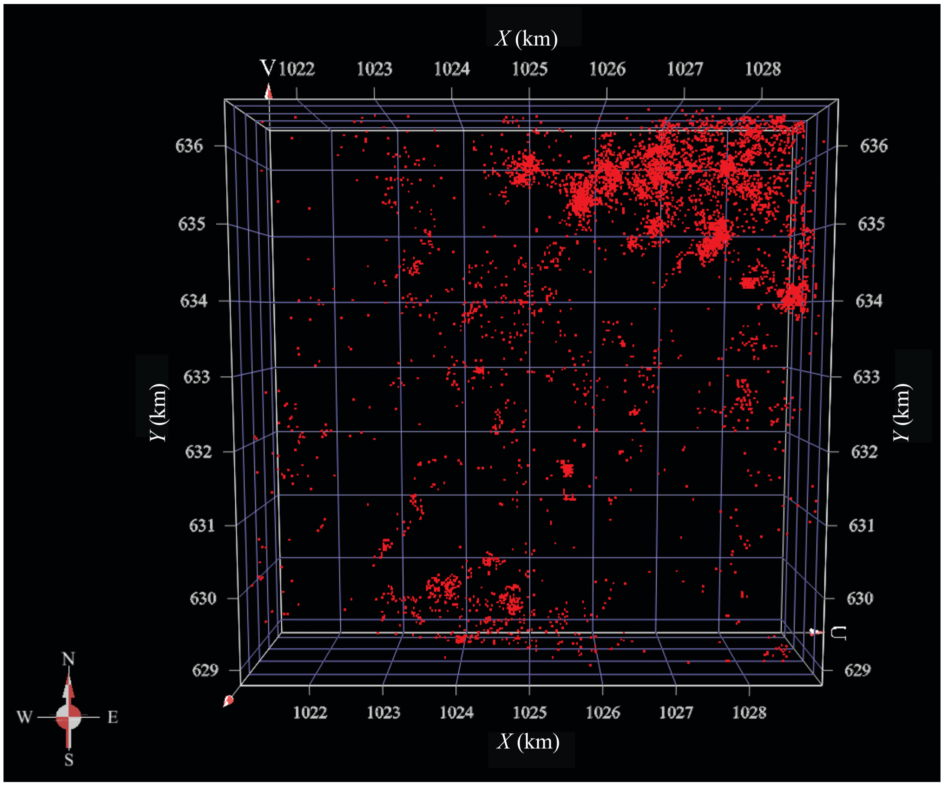

Figure 12 Depositional model of the upper Cypress after a 90% cutoff was applied to make only the clean sandstone cells visible. The model is mostly shale with a scattering of clean cells. Northeast–southwest-trending lenses are visible in the northeastern corner, which corresponds to the transition to Noble North Field. V, north; U, east.

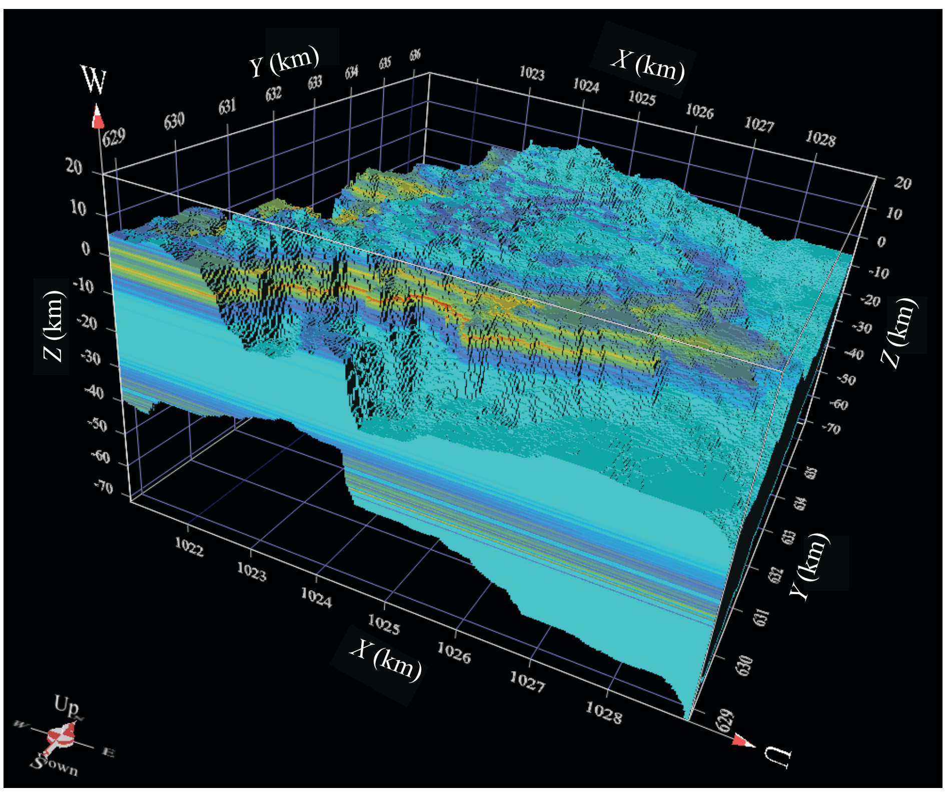

Figure 13 The diagenetic model. Warm colors indicate high odds of encountering the low-porosity facies, whereas cool colors indicate low odds. The low-porosity facies are mostly found in two distinct bands interpreted as calcite cement at the oil–water contact and 9 ft (3.3 m) below the oil–water contact. The low-porosity facies also occur near the base of the model and are caused by shale appearing in some logs where the sandstone transitions to shale at the base of the thick Cypress. 50× vertical exaggeration. W, up; U, east.

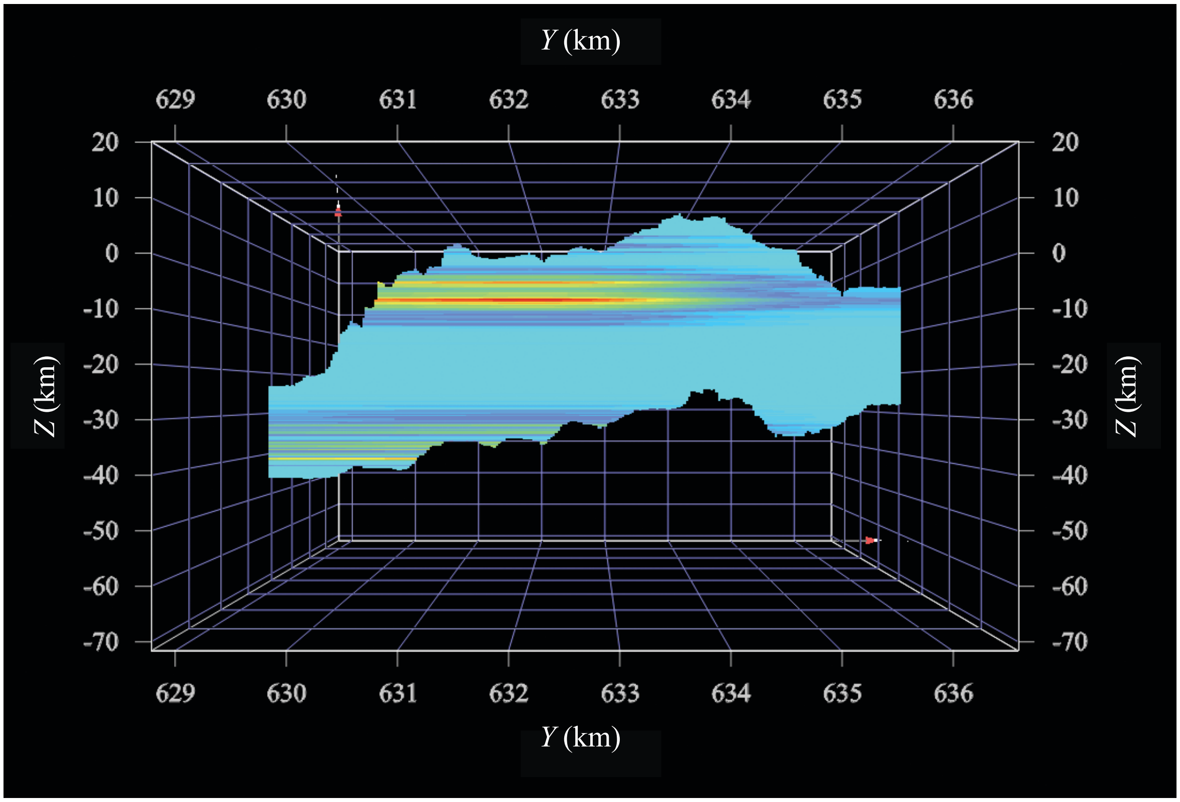

Figure 14 North–south-oriented slice of the diagenetic model. Warm colors indicate better odds of encountering low-porosity facies. The calcite cement appears as two parallel layers of low-porosity facies in the upper reservoir. The model has been flattened on the oil–water contact, so the upper layer occurs at the contact. The lower band is more pronounced and occurs approximately 9 ft (3.3 m) below the oil–water contact. Both layers disappear near the northern edge. There is also a chance of encountering low-porosity facies, which are interpreted as discontinuous shale bodies, in the lower portion of the reservoir (>98 ft, or >30 m below the oil–water contact). 50× vertical exaggeration.

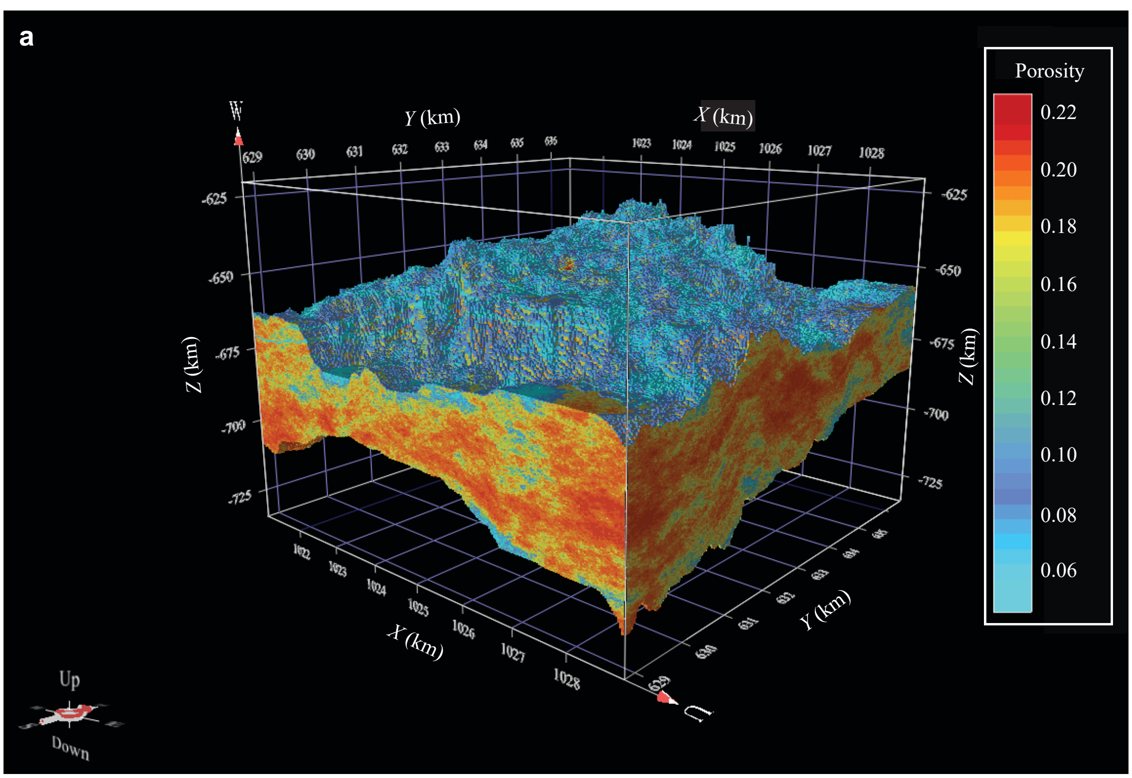

Figure 15 Final model of porosity (a) and permeability (b, p. 17). The upper boundary has a high shale content, which results in low porosity and permeability. The middle of the model is relatively clean sandstone with a typical porosity of 17% and permeabiltiy of 400 mD. W, up; U, east.

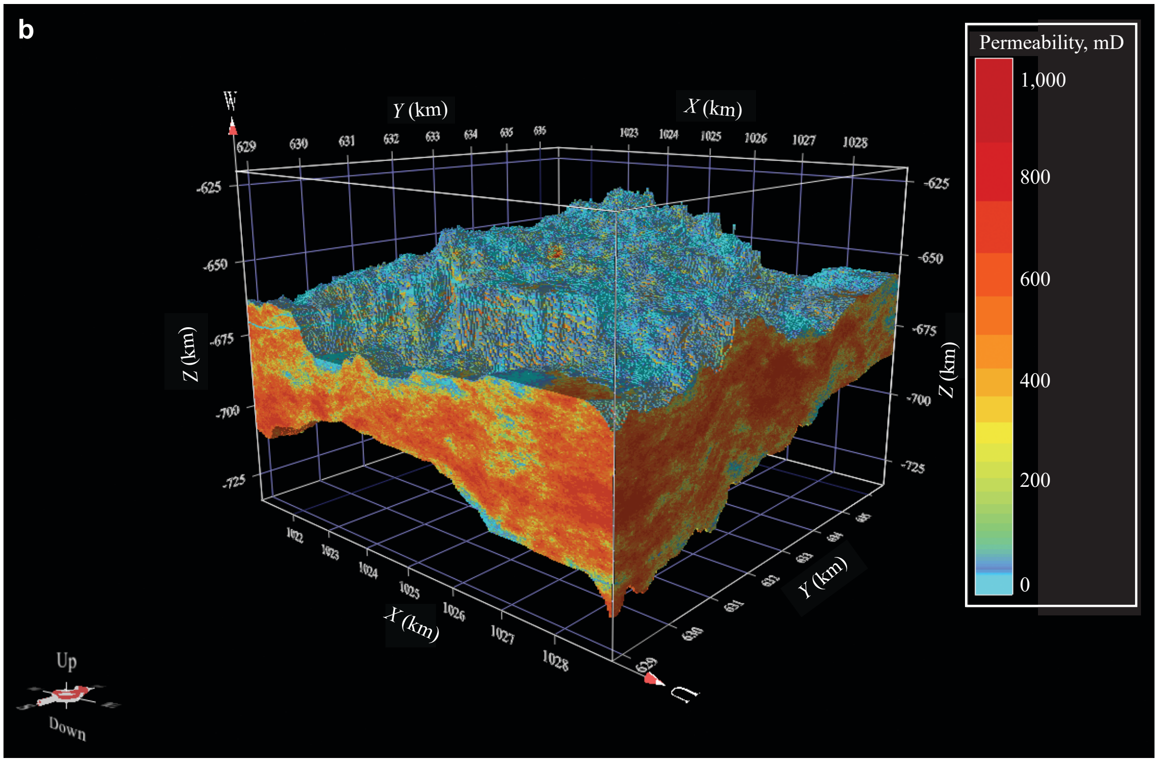

Figure 15 *Continued.*

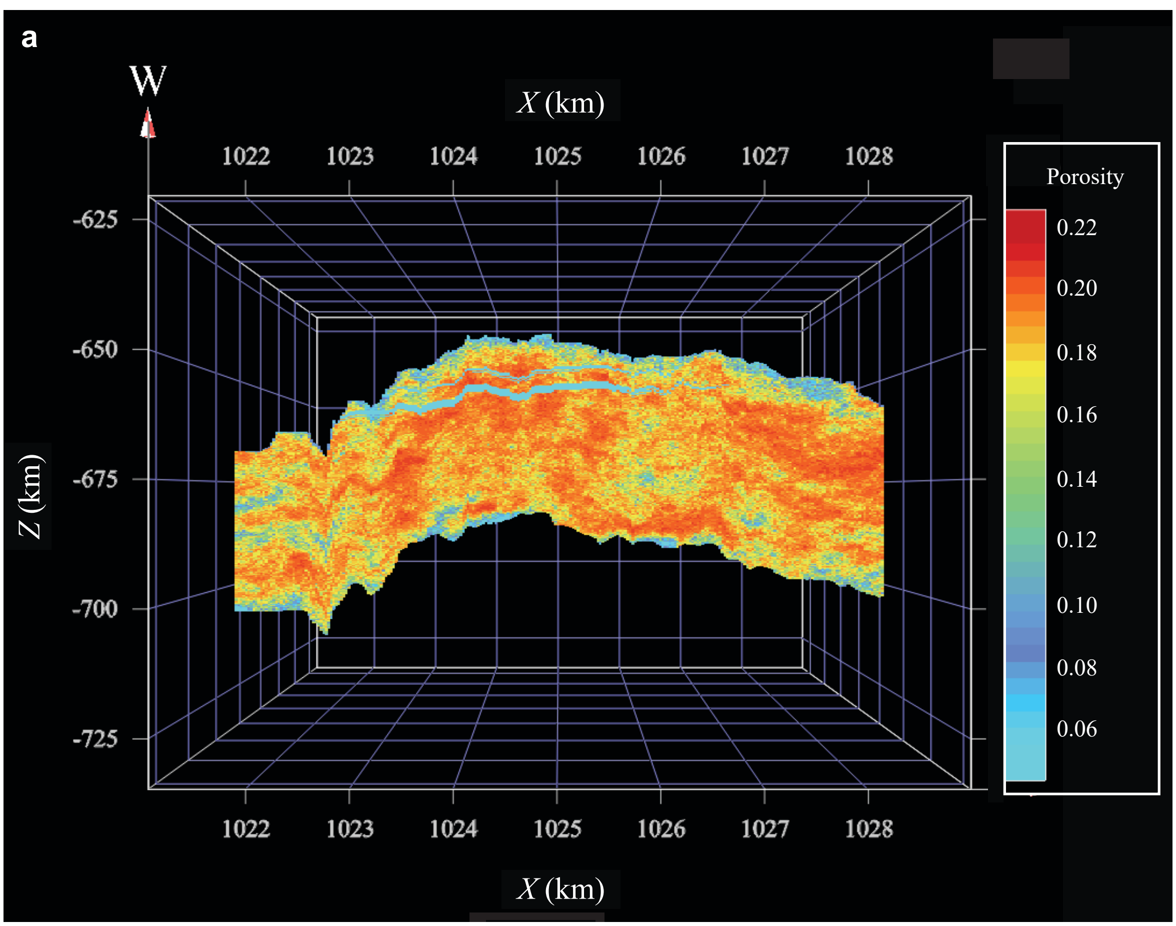

Figure 16 Slice from the middle of the final model showing the internal distribution of porosity (a) and permeability (b, p. 18). The view of the internal distribution reveals the stark contrast between clean sandstone and the two parallel layers of cement in the upper reservoir. This slice is from approximately the middle of the model (10,000 ft, or 3,048 m from the southern boundary) and is shown with a 50× vertical exaggeration. W, up.

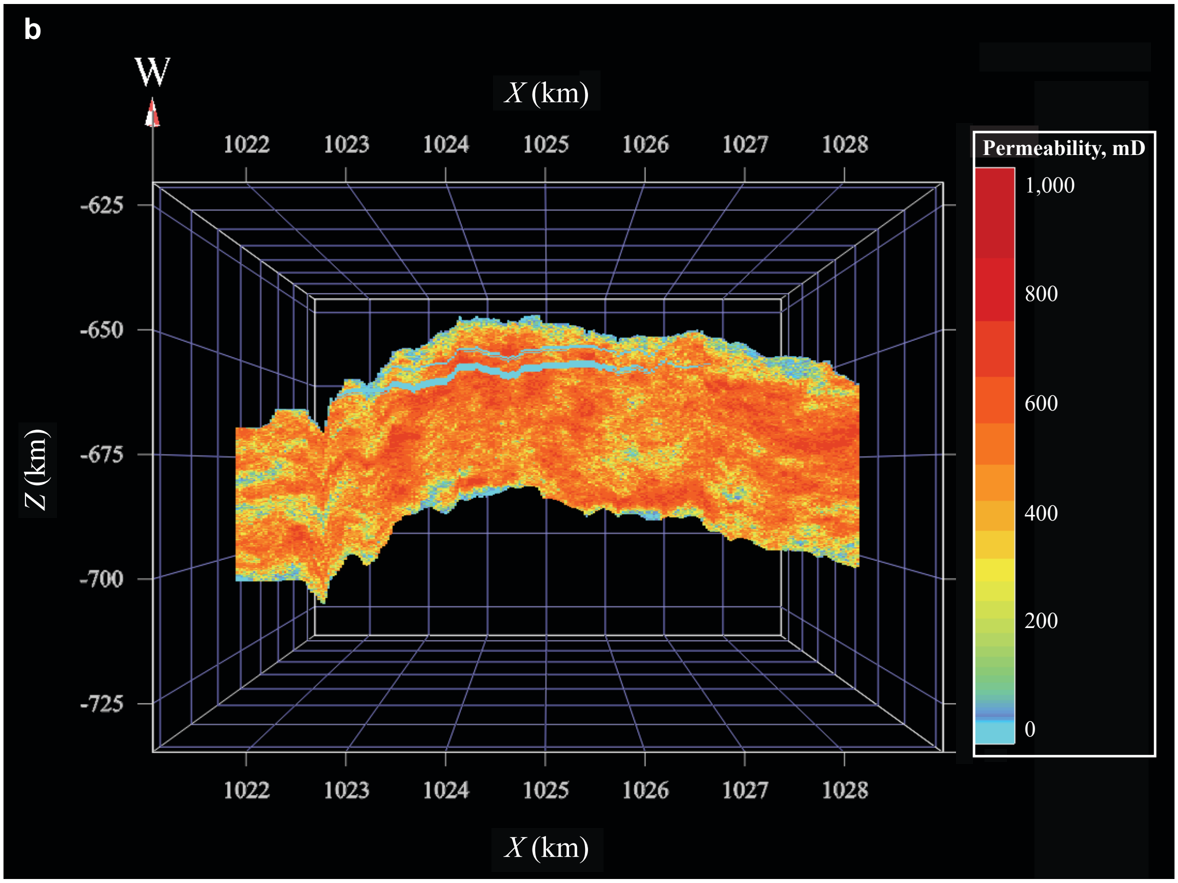

Figure 16 *Continued.*

Combined Model Results

The final combined model integrates the porosity and permeability based on the normalized SP values simulated in the depositional model with two bands of calcite cement from the diagenetic model. Figures 15 and 16 show the distribution of the petrophysical properties, and Table 6 lists the statistics for the final model. This model reflects the heterogeneity and internal architecture of the sandstone presented in the geologic conceptual model of Webb and Grigsby (2020).

CONCLUSIONS

This study demonstrates that detailed geologic characterization is critical when constructing a robust and representative geocellular model. In this case, understanding the geology of the Cypress Sandstone played a role in three key areas: (1) delineating bed boundaries to separate the model into discrete, genetically related elements based on lithofacies; (2) incorporating reservoir heterogeneity in the form of diagenetic calcite cement within an otherwise lithologically homogeneous sandstone; and (3) assigning core analysis data to the proper facies so that it could be applied correctly to the model.

Separating the thick Cypress Sandstone from the upper shaley Cypress was necessary to detect anisotropy and transitional behavior within the thick Cypress and to construct accurate porosity-to-permeability transforms for each unit. Analysis of the core data revealed that each unit had a distinct porosity-to-permeability relationship and that points near (within 10 ft, or 3 m, of) the facies boundary occurred in both trends (Figure 9b). Averaging data for each core revealed that data within 10 ft (3 m) of the boundary fell into the high-permeability trend of the thick Cypress in some wells and into the lower permeability trend of the upper Cypress in others. This result suggests that the transition from clean sandstone in the thick Cypress to shale in the upper Cypress is abrupt in some wells (resulting in points near the boundary occurring within the high-permeability trend) and more gradual in others (resulting in points near the boundary occurring within the low-permeability trend). Furthermore, the final model reflects this behavior via shaley areas in the uppermost cells of the thick Cypress.

The calcite cement identified in the core analysis is believed to form a continuous baffle to fluid flow in the vicinity of the oil–water contact. A conceptual framework for understanding what this cement is, how it formed, and how it affected wireline logs was necessary to identify and properly incorporate it into the model. The calcite cement was not detected by SP logs. This necessitated using neutron-density porosity logs to incorporate calcite cement into the model, which complicated the normalized SP-to-porosity transform. Because

Table 6 Statistics from the embedded model[1]

Attribute	Model value
Number of cells	
Total	1,980,160
Defined	734,180
x	130
y	128
z	119
Spacing, ft (m)	
x/*y*	200 (61)
z	3 (0.9)
Elevation (subsea), ft (m)	
Minimum	–2,054 (626)
Maximum	–2,411 (735)
Thickness, ft (m)	
Minimum	45 (14)
Maximum	189 (58)
Mean	130 (40)
Porosity	
Minimum	0.04
Maximum	0.21
Mean	0.17
Median	0.18
Standard deviation	0.04
Horizontal permeability, mD (μm^2)	
Minimum	2.85 (0.00)
Maximum	689.47 (0.68)
Mean	401.56 (0.40)
Median	456.35 (0.45)
Standard deviation	186.90 (0.18)
Vertical permeability, mD	
Minimum	0.41 (0.00)
Maximum	371.55 (0.37)
Mean	159.22 (0.16)
Median	173.44 (0.17)
Standard deviation	104.07 (0.10)

the cement did not produce a response on the SP log, data points from the normalized SP and neutron-density porosity logs that fell within the calcite-cemented zone needed to be identified and removed. This was done to understand the relationship between normalized SP and porosity in the unaltered sandstone (Figure 8). Failing to do so would have increased scatter and may have resulted in an erroneous SP-to-porosity transform.

The calcite cement baffle demonstrates the importance of understanding the mechanism responsible for creating geologic features when selecting a datum. Because the calcite cement is a diagenetic (instead of depositional) feature, data needed to be flattened along the oil–water contact (the plane in which the diagenesis occurred) to properly detect trends. Shifting the data to stratigraphic space by using a geologic datum would have made the lateral continuity of the baffle difficult to detect and would have resulted in a model with a zone of discontinuous cement.

ACKNOWLEDGMENTS

This research was funded in part by the U.S. Department of Energy under contract number DE-FE0024431. Portions of the mapping were conducted with IHS Petra software as part of the University Grants Program. Geocellular models, including variogram analysis and model images, were created with Geovariances ISATIS software. The authors extend thanks to Robert Ritzi and Hannes Leetaru for their contributions to and review of this manuscript. Daniel Klen and Susan Krusemark provided technical editing of this manuscript, and Michael Knapp assisted with final layout.

REFERENCES

Blunt, M., F.J. Fayers, and F.M. Orr Jr., 1993, Carbon dioxide in enhanced oil recovery: Energy Conversion and Management, v. 34, no. 9–11, p. 1197–1204.

Hill, B., S. Hovorka, and S. Melzer, 2013, Geologic carbon storage through enhanced oil recovery: Energy Procedia, v. 37, p. 6808–6830.

Kovscek, A.R., and M.D. Cakici, 2005, Geologic storage of carbon dioxide and enhanced oil recovery. II. Cooptimization of storage and recovery: Energy Conversion and Management, v. 46, no. 11–12, p. 1941–1956.

Leetaru, H.E., 1990, Application of old electric logs in the analysis of Aux Vases Sandstone (Mississippian) reservoirs in Illinois: Illinois State Geological Survey, Illinois Petroleum 134, 21 p.

Webb, N.D., and N.P. Grigsby, 2020, Assessing the Cypress Sandstone for carbon dioxide-enhanced oil recovery and carbon storage: Part I—Reservoir characterization of noble oil field, western Richland County, Illinois: Illinois State Geological Survey, Circular 601, 53 p.